

# RSC Advances



This is an *Accepted Manuscript*, which has been through the Royal Society of Chemistry peer review process and has been accepted for publication.

*Accepted Manuscripts* are published online shortly after acceptance, before technical editing, formatting and proof reading. Using this free service, authors can make their results available to the community, in citable form, before we publish the edited article. This *Accepted Manuscript* will be replaced by the edited, formatted and paginated article as soon as this is available.

You can find more information about *Accepted Manuscripts* in the [Information for Authors](#).

Please note that technical editing may introduce minor changes to the text and/or graphics, which may alter content. The journal's standard [Terms & Conditions](#) and the [Ethical guidelines](#) still apply. In no event shall the Royal Society of Chemistry be held responsible for any errors or omissions in this *Accepted Manuscript* or any consequences arising from the use of any information it contains.



# AgBr Nanoparticles Decorated BiPO<sub>4</sub> Microrod: A Novel *p-n* Heterojunction with Enhanced Photocatalytic Activities

Cite this: DOI: 10.1039/x0xx00000x

Danjuan Wang\*, Linlin Yue, Li Guo, Feng Fu\*, Xiaomei He, Huidong Shen

AgBr nanoparticles loaded BiPO<sub>4</sub> microrods have been successfully synthesized via a facile deposition-precipitation method. XRD, FE-SEM, TEM, EIS, UV-Vis-DRS techniques were employed to characterize the phase composition, morphology and light absorption properties of the as-synthesized samples. Methylene blue (MB) and Phenol(Ph) were selected as a model pollutant to investigate the photocatalytic activity of the as-synthesized samples under visible-light irradiation. The experimental results show that different amount of AgBr on BiPO<sub>4</sub> exhibit an obvious effect on the degradation of MB and the optimum molar ratio of AgBr and BiPO<sub>4</sub> is 1:10. In particular, the photocatalytic activity of AgBr/BiPO<sub>4</sub> is superior to the activities of two individual photocatalyst, indicating the presence of a synergic effect between two component in AgBr/BiPO<sub>4</sub>. On the basis of photocatalytic results and energy band diagram, the activity enhancement mechanism of AgBr/BiPO<sub>4</sub> composite has also been investigated. The p-type semiconductor AgBr and n-type semiconductor BiPO<sub>4</sub> can match each other and form a novel p-n heterojunction, thus increasing the photogenerated electron-hole pair separation efficiency. Therefore, this work provides some help for the design of novel and efficient BiPO<sub>4</sub>-based photocatalyst with multi-components for enhancing visible-light-driven photocatalytic activity.

Received 00th xxxx 2015,  
Accepted 00th xxxx 2015

DOI: 10.1039/x0xx00000x

www.rsc.org/

## 1 Introduction

During the past few decades, photocatalysis has stimulated great interest in the field of environmental protection and energy conversion because organic pollutants can be degraded completely and water can be decomposed into oxygen and hydrogen by some semiconductors under light irradiation.<sup>1-4</sup> Different kinds of semiconductors have been used as photocatalysts to initiate reactions at their interface. Among such photocatalysts, TiO<sub>2</sub> has been proved to be an excellent photocatalyst for environmental remediation owing to its high potential, physical and chemical stability, nontoxicity and inexpensiveness.<sup>5-8</sup> However, the practical application of TiO<sub>2</sub>-based photocatalyst is limited for several reasons. First, TiO<sub>2</sub> is a semiconductor with wide band gap ( $E_g \approx 3.2$  eV) and only been excited by UV-light which merely accounts for around 4% of the received solar energy. Second, the high recombination rate of photogenerated electron/hole pairs results in the low photon utilization efficiency and slow photooxidation rate. Therefore, many scholars have focused on the search for utilizing visible light by doping with hybrid atoms and coupling with other low energy gap semiconductors.<sup>9</sup>

It is well known that the photocatalytic process involves the generation of charge carriers such as electrons and holes induced by light irradiation. And ideal photocatalysts should have both wide wavelength range of exciting light and low recombination rate of photogenerated charge carriers. Therefore, it is necessary to develop effective ways to improve the charge separation efficiency and extend the spectral responsive range. The ideal of forming a heterojunction structure between wide bandgap photocatalyst and narrow bandgap semiconductor with matched band potentials is proven effective. Recently, *p-n* heterojunction nanostructures have attracted considerable attention due to their unique optical, optoelectronic and electronic properties.<sup>10-14</sup>

Among such photocatalysts, many Bi-based photocatalytic materials have been reported with several advantages as photocatalyst over the competing materials.<sup>15</sup> Being one of the most important multifunctional materials, Bismuth phosphate (BiPO<sub>4</sub>) has received particular attention recently because of its excellent photocatalytic property.<sup>16-42</sup> BiPO<sub>4</sub> photocatalysts has an optical indirect band gap of 3.85 eV, which exhibits high photocatalytic oxidative ability for organic dye decomposition.<sup>27-28</sup> Zhu et al. have reported that the photocatalytic activity of BiPO<sub>4</sub> is twice that of TiO<sub>2</sub> (P25, Degussa), while the BET surface of BiPO<sub>4</sub> is just one tenth of that of P25.<sup>28</sup> Unfortunately, there are two mainly drawbacks in the application of BiPO<sub>4</sub> photocatalyst. Firstly, bare-BiPO<sub>4</sub> exhibits photocatalytic activity under UV-light irradiation which merely accounts for around 4% of the received solar energy. Secondly, the rapid recombination of photoinduced electron and hole pairs seriously limits the light energy conversion

College of Chemistry & Chemical Engineering, Yan'an University, Shaanxi Key Laboratory of Chemical Reaction Engineering, Yan'an 716000, China. E-mail: wangdj761118@163.com; yadxfufeng@126.com; +86-911-2586217

efficiency. Therefore, the way to broaden the range of absorption spectra and enhance the separation of photogenerated carriers of BiPO<sub>4</sub> is important in maximizing the photocatalytic efficiency. In recent years, many strategies have been adopted to overcome the intrinsic limitation of BiPO<sub>4</sub>. One strategy is to design and controllable-synthesis of BiPO<sub>4</sub>.<sup>16-30</sup> Other effects have been made, such as metal elements doping<sup>31-34</sup> and surface noble-metal modification.<sup>35-36</sup> Besides these, design and fabrication of heterostructured BiPO<sub>4</sub> with different carriers or different band gap has turned to be another effective approach.<sup>37-42</sup> To this end, we intended to design heterojunction by coupling BiPO<sub>4</sub> with a p-type narrow-band-gap semiconductor with matched potentials. The well-fabricated BiPO<sub>4</sub>-based p-n heterojunction could restrict the recombination of charge carriers and enhance the quantum yield. The photoinduced electron can transfer from p-type semiconductor to BiPO<sub>4</sub>, which favors the charge separation and also improve the visible-light utilization efficiency.

silver bromide (AgBr) with a narrow band gap (2.6 eV), is an important photosensitive semiconductor. Under solar irradiation AgBr can absorb photons to generate electrons and holes. Thus AgBr is also a potential photocatalyst. But the photoinduced electrons will combine with interstitial Ag<sup>+</sup> ions to form an Ag<sup>0</sup> cluster, which leads to photodecomposition of AgBr. So, the instability of pure AgBr is a obstacle in practical photocatalytic application. As reported in previous work by Li and coworker, AgBr/BiPO<sub>4</sub> composite was synthesized through hydrothermal method in [C<sub>16</sub>min]Br ionic liquid and exhibits higher photocatalytic activity than that of pure BiPO<sub>4</sub> under UV light irradiation.<sup>42</sup> Although the UV-responsive photocatalytic property of AgBr/BiPO<sub>4</sub> composite was confirmed and well-studied, the 1D AgBr/BiPO<sub>4</sub> have never been constructed. Very recently, our group has successfully synthesized 3D nest-like Bi<sub>2</sub>WO<sub>6</sub> by a hydrothermal method without any additives, and AgBr quantum dots (QDs) were decorated on the surface of Bi<sub>2</sub>WO<sub>6</sub> to form a novel p-n heterojunction via a followed facile precipitation-deposition process.<sup>43</sup> In current work, the novel one-dimensional (1D) AgBr/BiPO<sub>4</sub> p-n heterojunction photocatalyst was designed and fabricated using the same strategy. AgBr nanoparticles were deposited on the surface of one-dimensional rod-like BiPO<sub>4</sub> microcrystals with a very close combination. MB and phenol were utilized as model pollutants to examine the photocatalytic activity of the as-fabricated AgBr/BiPO<sub>4</sub> heterojunctions under visible-light irradiation. AgBr nanoparticles greatly enhance the photocatalytic activity of 1D rod-like BiPO<sub>4</sub> in photocatalytic degradation of organic pollutants. It was also found that the organic pollutants can be directly oxidized by both h<sub>VB</sub><sup>+</sup> and ·OH radicals in the present of AgBr/BiPO<sub>4</sub> photocatalyst system. As the heterojunction at the interface can facilitate the separation of charge carriers, this can also help to determine which carriers, photogenerated electrons or holes, play a major role in the photocatalysis. We believe that this work maybe help to develop new photocatalysts for the photodegradation of MB and phenol, as well as to understand the photocatalytic mechanism better than before.

## 2 Experimental Section

### 2.1. Chemicals and materials

All reagents were analytically pure and were used without further purification. Bismuth nitrate pentahydrate (Bi(NO<sub>3</sub>)<sub>3</sub>·5H<sub>2</sub>O), ammonium bihydrogen phosphate (NH<sub>4</sub>H<sub>2</sub>PO<sub>4</sub>), potassium bromide (KBr), Silver nitrate (AgNO<sub>3</sub>), ammonia solution, phenol (C<sub>6</sub>H<sub>5</sub>OH), methylene blue (MB), and nitric acid (HNO<sub>3</sub>) were obtained from Sinopharm Chemical Reagent Co., Ltd. Deionized water was used throughout this study.

### 2.2 Preparation of AgBr/BiPO<sub>4</sub> photocatalyst

**Preparation of pure-BiPO<sub>4</sub> photocatalyst.** Using equal moles of Bi(NO<sub>3</sub>)<sub>3</sub>·5H<sub>2</sub>O and NH<sub>4</sub>H<sub>2</sub>PO<sub>4</sub>, Bismuth phosphate (BiPO<sub>4</sub>) rod-like microcrystals were successfully synthesized via a simple hydrothermal process. In a typical process, 5mmol Bi(NO<sub>3</sub>)<sub>3</sub>·5H<sub>2</sub>O was dissolved in 5mL 4mol/L HNO<sub>3</sub> in advance, then NH<sub>4</sub>H<sub>2</sub>PO<sub>4</sub> solution (5mmol NH<sub>4</sub>H<sub>2</sub>PO<sub>4</sub> was dissolved in 15mL distilled water) were slowly added Bi(NO<sub>3</sub>)<sub>3</sub> solution drop-wise under vigorously stirring. The mixture was vigorously stirred for 30min at room temperature. Afterward, the suspension was transport into 50mL Teflon-lined autoclave. Then, the autoclave was sealed in a stainless steel tank and heated at 190°C for 24h. After hydrothermal reaction, the autoclave was naturally cooled to room temperature. The resulting precipitates were collected, washed with deionized water and absolute ethanol for several times, and dried in a vacuum oven at 80°C for 4h.

**Preparation of AgBr/BiPO<sub>4</sub> heterojunction photocatalyst.** Firstly, a certain amount of as-synthesized BiPO<sub>4</sub> powder was dispersed into deionized water. Then, a certain volume of Ag (NH<sub>3</sub>)<sub>2</sub><sup>+</sup> solution were added into above solution under vigorously stirring. Afterwards, a certain volume of KBr solution was added dropwise into the above mixture with stirring for another 4 hours. The resulting precipitates were collected, washed with deionized water and absolute ethanol, and the products were dried in a vacuum oven at 80 °C for 4h. The obtained grey sample was collected with different mole ratio of AgBr to BiPO<sub>4</sub> by adjusting the added amount of Ag (NH<sub>3</sub>)<sub>2</sub><sup>+</sup> and KBr solution. For comparison, pure-AgBr was also synthesized by the following process. 10.6169g AgNO<sub>3</sub> was dissolved in 24.31mL ammonia solution (28%), and then diluted with deionized water to 250mL silver ammonia (Ag(NH<sub>3</sub>)<sub>2</sub><sup>+</sup>) solution. 1.1902g KBr was dissolved in 40mL deionized water. Then, took 40ml (Ag (NH<sub>3</sub>)<sub>2</sub><sup>+</sup>) solution into a small beaker, and the prepared KBr solution was added dropwise into the beaker with stirring. The mixture was vigorously stirred for 8h. Subsequently the resulting precipitates were collected, washed with deionized water and absolute ethanol, and the products were dried in a vacuum oven at 80°C for 4h.

### 2.3 Characterization of AgBr/BiPO<sub>4</sub> photocatalyst

X-ray Powder diffraction (XRD) was carried out with a Shimadzu XRD-7000 X-ray diffractometer using CuKα radiation (λ = 0.15418 nm) with a scanning rate of 2°·min<sup>-1</sup> in the 2θ range from 20° to 80. The Brunauer-Emmett-Teller (BET) specific surface area (S<sub>BET</sub>) of the samples were measured by nitrogen adsorption in an ASAP2010 Micromeritics Instrument Corporation. X-ray photoelectron spectroscopy (XPS) images were recorded on a PHI-5400 X-ray photoelectron spectrometer. The field emission scanning electron microscope (FE-SEM) images were taken on a JSM-6700F scanning electron microscope. High-resolution transmission electron (HR-TEM) images and selected area electron diffraction (SAED) were recorded on a JEM-2100 electron microscope at an accelerating voltage of 200 kV. The UV-Vis diffuse reflectance spectra (UV-Vis-DRS) of the samples were obtained using Shimadzu UV-2550 UV-Visible spectrophotometer. BaSO<sub>4</sub> was used as a reflectance standard.

### 2.4. Photocatalytic activities test

The photocatalytic activities of AgBr/BiPO<sub>4</sub> were evaluated by degradation of Methyl-Blue (abbreviated as MB) and phenol (Ph), using 400W halogen lamp as light source. In each experiment, a certain amount of photocatalyst was added into MB or Ph aqueous solution. A series of 50 mL quartz tubes of 2.0 cm diameter were used as the reaction vessel. The

temperature of the reaction solution was maintained at approximately 25 °C to avoid temperature effects in the reaction. Prior to illumination, the suspension was magnetically stirred in dark for 90min to ensure that an adsorption/desorption equilibrium was established between the photocatalyst and the target organic pollutant. At every irradiation time interval of 10 min, took out one of quartz tube, then centrifuged (9000 rpm, 6min) to remove the photocatalyst particles. The catalyst-free solution was analyzed by recording variations at the wavelength of maximal absorption in the UV-Vis spectra of MB with a UV-2550(Shimadzu, Japan)spectrophotometer. The concentration of dye was determined by its maximum absorption for MB with deionized water as a reference sample. The concentration of phenol was determined by using 4-aminoantiphtine spectrophotometric method (Chinese HJ 503-2009). Chemical oxygen demand(COD) was determined at a COD rapid monitor(5B-3B, LanHua co., LTD, China).

To investigate the transition of photogenerated electrons before and after AgBr, BiPO<sub>4</sub> and AgBr/BiPO<sub>4</sub> electrodes were prepared as follows: 5 mg of photocatalyst was suspended in 10 mL ethanol to produce slurry, which was then spread on a 2cm×1.5cm indium-tin oxide (ITO) glass electrode. Electrodes were exposed to UV light for 1h to eliminate ethanol and subsequently calcined at 120 °C for 5h. The photoelectric performance were measured on an electrochemical system(CHI-600b, China). A standard three-electrode cell with a working electrode, and a standard calomel electrode (SCE) as reference was used in photoelectric studies. And 0.1mol·L<sup>-1</sup> Na<sub>2</sub>SO<sub>4</sub> was used as electrolyte solution. Potentials are given with UV light(or visible light) on and off were measured at 0.0V. Electrochemical impedance spectra (EIS) were recorded in the open circuit potential mode.

### 3 Results and discussion

#### 3.1 Phase composition and morphology of samples.

Fig. 1 shows the typical XRD patterns of the as-synthesized pure-BiPO<sub>4</sub>, AgBr and AgBr/BiPO<sub>4</sub> heterojunction with different

AgBr contents. Fig. 1a is the XRD pattern of pure BiPO<sub>4</sub>, and it can be seen that all the peaks almost coincide with the Bragg reflections of standard BiPO<sub>4</sub> structure (JCPDS 89-0287) without any impurity phase, and can be indexed to the monoclinic phase BiPO<sub>4</sub>. Fig. 1f reveals that the position of the main characteristic diffraction is fully fitted with face-centered cubic AgBr (JCPDS NO. 79-0149). Fig. 1b-1e shows the XRD patterns of AgBr/ BiPO<sub>4</sub> with different composition. From those XRD patterns, we can see that the samples have two sets of characteristic diffraction peak corresponding to the face-centered cubic crystal system AgBr and monoclinic crystal system BiPO<sub>4</sub> and without any new phase is detected. As compared with the pure BiPO<sub>4</sub> crystals, small diffraction peaks of the AgBr crystals have been detected. In Fig. 1b-1e the peaks at  $2\theta = 26.72^\circ$ ,  $30.96^\circ$  and  $44.34^\circ$  were assigned to (111), (200) and (220) crystal planes of AgBr (JCPDS NO. 79-0149), respectively, confirming that AgBr has formed on the surface of the sample. With the increasing AgBr content, the intensity of diffraction peaks of AgBr increases. The above results reveal the coexistence of BiPO<sub>4</sub> and AgBr.

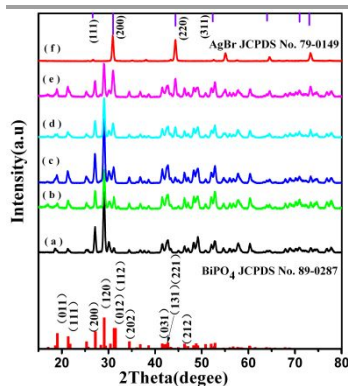


Fig. 1 XRD patterns of as-prepared samples: (a) BiPO<sub>4</sub>, (b) 5at%AgBr/BiPO<sub>4</sub>, (c)10at%AgBr/BiPO<sub>4</sub>, (d)14.6at%AgBr/ BiPO<sub>4</sub>, (e) 20at%AgBr/ BiPO<sub>4</sub>; (f) pure-AgBr.

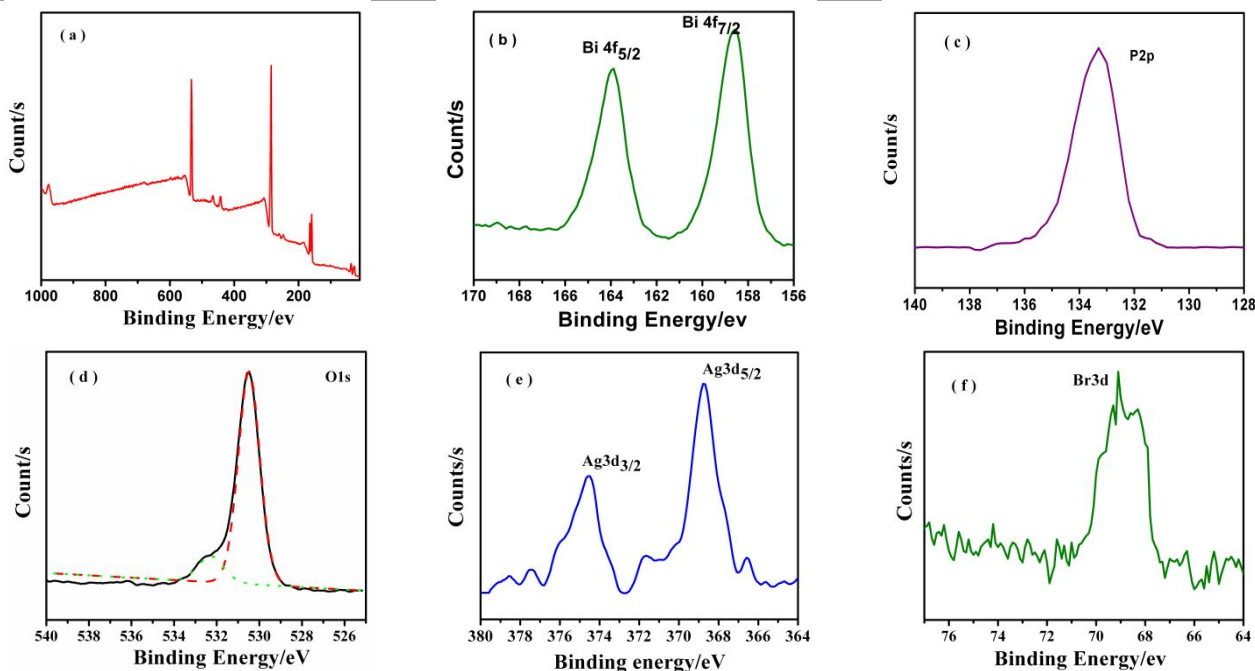
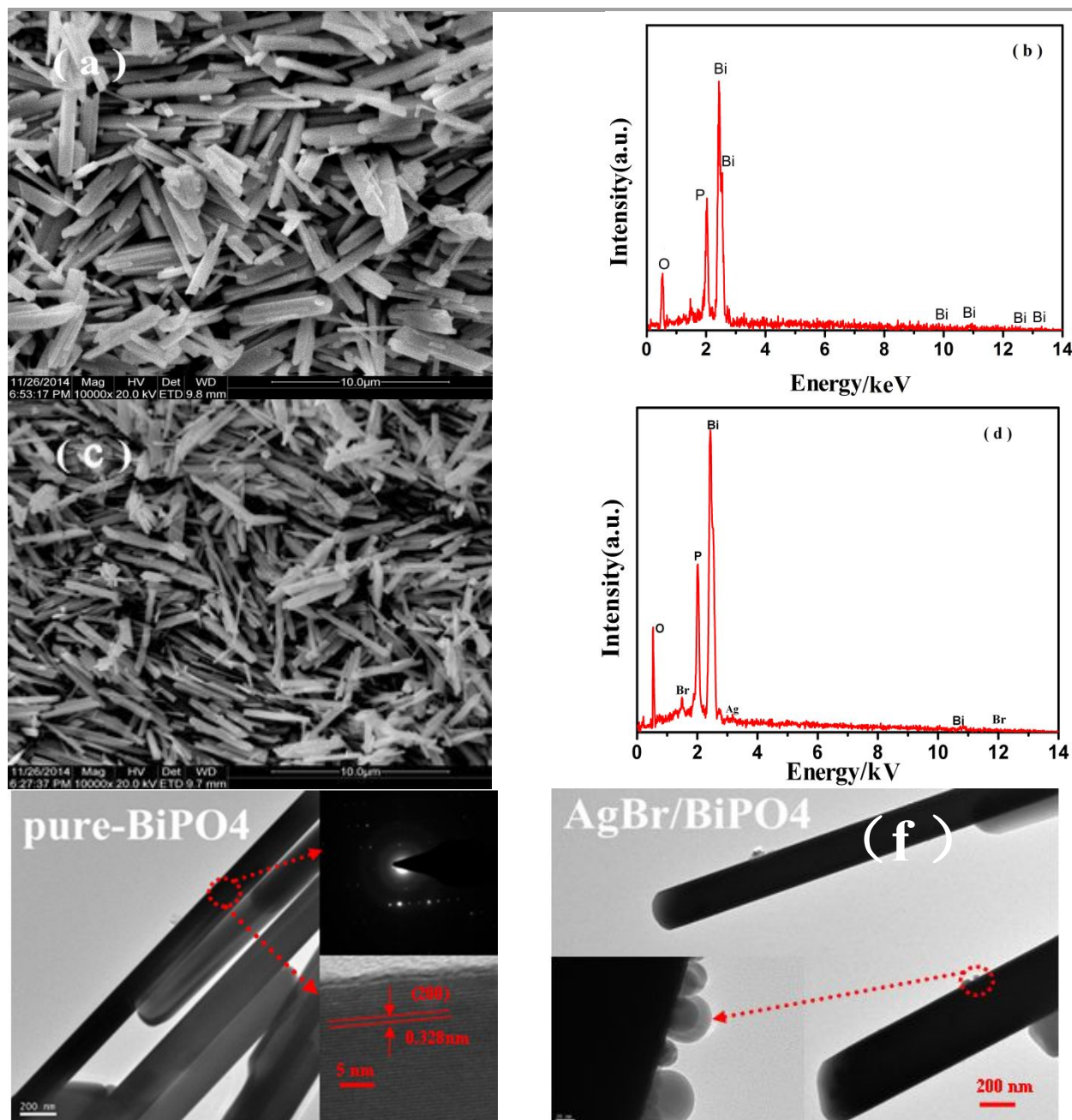


Fig. 2 XPS spectra of 10at%AgBr/ BiPO<sub>4</sub>. (a) The survey spectra; (b) Bi4f; (c) P2p, (d) O1s, (e) Ag3d, (f) Br3d.





**Fig. 3** SEM and TEM images and corresponding EDS of the samples. (a) SEM image of  $\text{BiPO}_4$ ; (b) EDS of  $\text{BiPO}_4$ ; (c) SEM image of 10at%AgBr/ $\text{BiPO}_4$ ; (d) EDS of AgBr/ $\text{BiPO}_4$ ; (e) TEM picture of  $\text{BiPO}_4$ ; (f) TEM picture of AgBr/ $\text{BiPO}_4$  heterojunction.

Further evidence for the chemical composition and oxidation states of the as-prepared 10at%AgBr/ $\text{BiPO}_4$  was obtained by XPS technique (Fig. 2). It can be seen that the sample contains only Bi, W, O, Ag, Br elements and a trace amount of carbon. The C element ascribed to the residual carbon from the precursor solution and the adventitious carbon from the XPS instrument itself (Fig. 2a). Fig. 2b-2f show the high-resolution spectra of the Bi 4f, P 2p, O 1s, Ag 3d and Br 3d regions, respectively. In Fig. 2b, two peaks at 159 eV and 164 eV are attributed to  $\text{Bi } 4f_{7/2}$  and  $\text{Bi } 4f_{5/2}$  of  $\text{Bi}^{3+}$  in 14.6at%AgBr/ $\text{BiPO}_4$ .<sup>43</sup> Peak at 133.32 eV, as shown in Fig. 2c, can be ascribed to a  $\text{P}^{5+}$  oxidation state in  $\text{BiPO}_4$ .<sup>44</sup> As shown in Fig. 2d, the asymmetric XPS of O 1s may be fitted into two kinds of

chemical states: crystal lattice oxygen and adsorbed oxygen.<sup>17</sup> Fig. 2e gives the high-resolution XPS spectrum of Ag 3d. The  $\text{Ag } 3d_{3/2}$  and  $\text{Ag } 3d_{5/2}$  peaks are identified at 3740.0 and 368.0 eV, respectively, suggesting the presence of  $\text{Ag}^+$ .<sup>45</sup> Moreover, in Fig. 2e the peak of Br 3d at 69.07 eV is due to the crystal lattice of Br<sup>-</sup> in AgBr.<sup>43,46</sup> Therefore, according to XPS and XRD investigation, the results confirmed that there were both  $\text{Bi}_2\text{WO}_6$  and AgBr species in the 10at%AgBr/ $\text{BiPO}_4$  sample.

The size and morphology of as-synthesized samples was obtained by SEM, as shown in Fig. 3. It can be seen that pure- $\text{BiPO}_4$  exhibits a uniform one-dimensional (1D) rod-like microcrystal with the length of about 5  $\mu\text{m}$  (Fig. 3a). When AgBr

was deposited on the surface of 1D rod-like BiPO<sub>4</sub> microcrystal via a facile precipitation-deposition process (Fig. 3c), the resulted AgBr/BiPO<sub>4</sub> composite sample exhibits the similar morphology and size to that of pure BiPO<sub>4</sub>. Obviously, the coexistence of AgBr and BiPO<sub>4</sub> do not significantly affect their morphologies. Further information about AgBr/BiPO<sub>4</sub> microcrystals were obtained from TEM and HR-TEM images (Figs. 3e-3f). It can be seen that pure BiPO<sub>4</sub> microcrystals exhibit an uniform 1D rod-like microcrystals with smooth surface (Fig. 3e). The corresponding selected area electron diffraction (SAED) pattern (upper part of insert pictures in Fig. 3e) reveals the well-aligned clear diffraction spots that can be indexed to the monoclinic structure of BiPO<sub>4</sub>. The single crystal nature and parameters of rod-like BiPO<sub>4</sub> are also confirmed by HR-TEM (lower part of insert pictures in Fig. 3e). The space of the lattice fringes is found to be about 0.328 nm, as shown in Fig. 3e, which is in good agreement with the d-space of (200) planes of monoclinic structure of BiPO<sub>4</sub>. Furthermore, the locations of AgBr nanoparticles on the surface of rod-like BiPO<sub>4</sub> are pointed by arrow in TEM image (left of Fig. 3f). It reveals that some small spherical nanoparticles with size of about 20-30nm are highly dispersed on the surface of BiPO<sub>4</sub> and form the heterojunction structure, which is well consistent with the XRD and XPS results. Therefore, with the comprehensive analysis of the XRD, XPS, SEM, EDS and TEM investigation, the results confirm that there were both BiPO<sub>4</sub> and AgBr species in the heterojunction structure.

The EDS patterns of the 10at.%AgBr/BiPO<sub>4</sub> heterojunction (Fig. 3d) indicate that, besides Bi, P and O peaks, the Ag and Br diffraction peaks corresponding to AgBr are also observed, further confirming that the sample is composed of BiPO<sub>4</sub> and AgBr. The molar ratio of AgBr to BiPO<sub>4</sub> obtained in the powder is also close to the theoretical calculated value of AgBr/BiPO<sub>4</sub>. The molar ratio of the other samples analyzed by EDS was shown in Table 1. Also, as reported in Table 1, the specific surface area (S<sub>BET</sub>) of AgBr/BiPO<sub>4</sub> heterojunction slightly increased with the increasing of the content of AgBr.

Table 1. Physicochemical characterization of AgBr/BiPO<sub>4</sub> samples.

Sample	AgBr theoretical content (at.%)	AgBr experimental content (at.%)	S <sub>BET</sub> / (m <sup>2</sup> ·g <sup>-1</sup> )
Pure-BiPO <sub>4</sub>	0	0	3.55
5.0at%AgBr/BiPO <sub>4</sub>	5.0	4.84	3.60
10.0at%AgBr/BiPO <sub>4</sub>	10.0	9.36	3.72
14.6at%AgBr/BiPO <sub>4</sub>	14.6	14.24	3.76
20at%AgBr/BiPO <sub>4</sub>	20.0	19.28	3.85

### 3.2 Photoabsorption property of AgBr/BiPO<sub>4</sub> heterojunction

Fig. 4 shows the UV-Vis-DRS spectrum of pure-BiPO<sub>4</sub> and AgBr/BiPO<sub>4</sub> composites with different AgBr content. As revealed from Fig. 4, the absorption threshold values of the AgBr/BiPO<sub>4</sub> are extended to the visible light region in comparison with BiPO<sub>4</sub>. The absorption coefficient  $\alpha$  and band gap E<sub>g</sub> of direct transition semiconductor AgBr/BiPO<sub>4</sub> and BiPO<sub>4</sub> are related through the following equation:  $(\alpha h\nu)^2 = A(h\nu - E_g)$ , where  $h$  is Planck's constant,  $\nu$  is the light frequency, and  $A$  is a constant. According to equation (1), the band gap energy (E<sub>g</sub>) of

the resulting samples can be estimated by a plot of  $(\alpha h\nu)^2$  versus the photon energy ( $h\nu$ ).<sup>42-43</sup> The interception of the tangent to the X axis would give a good approximation of the E<sub>g</sub> of the samples (Fig. 4). Thus, the band gap of AgBr and BiPO<sub>4</sub> are estimated to 2.3eV and 3.45eV, respectively. They are slightly smaller than the reported values, which can be attributed to large crystal grain sizes and surface defects. After AgBr was loaded, the light absorption ability of AgBr/BiPO<sub>4</sub> with different AgBr content enhance obviously in the wavelength of 300-400nm and slightly in the visible-light region. the AgBr/BiPO<sub>4</sub> composites could absorb more photons than BiPO<sub>4</sub>. This should be attributed to the narrow band gap of AgBr, which is a p-type semiconductor with direct transition. The results of UV-Vis DRS suggest that the fabrication of the heterostructured AgBr/BiPO<sub>4</sub> composites can greatly improve the optical absorption property and increase the utilization of solar light, which are favorable for the enhancement of the photocatalytic activity.<sup>47-50</sup>

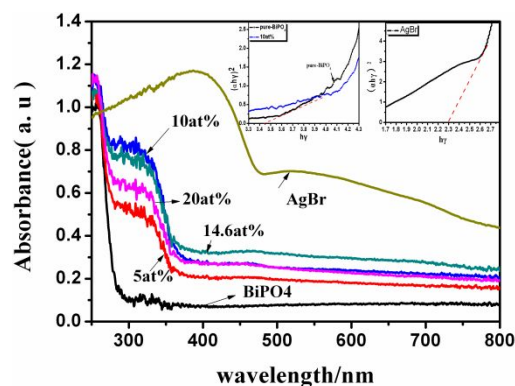


Fig. 4 UV-Vis-DRS spectrum of as-obtained samples.

### 3.4. Photocatalytic activity of AgBr/BiPO<sub>4</sub> photocatalyst

To investigate the visible-light catalytic activities of the samples, we chose the environment pollutant MB as the model pollutant, the metal halide lamp as the light source with a cutoff filter to remove the light below 420 nm and the photocatalytic degradation experimental results are shown in Fig 5 and Fig 6. Fig. 5a shows the photocatalytic degradation rate of MB under visible-light irradiation, where  $C$  is the concentration of MB at the wavelength of 665 nm and  $C_0$  is the concentration of MB after the adsorption equilibrium and before irradiation. Fig. 5b is UV-Vis absorption spectra of MB in the process of degradation by using 10.0at%AgBr/BiPO<sub>4</sub> as photocatalyst. By analyzing the change of concentration of MB solution vs illumination time, it is confirmed that MB photodegradation well obeys the pseudo-first-order kinetics model, i.e.  $\ln(C_t/C_0) = -kt$ , where  $C_t$  and  $C_0$  are the concentration of MB at time  $t$  and 0, respectively, and  $k$  is the pseudo-first-order rate constant. The rate constants  $k$  of MB photodegradation are derived from the  $\ln(C_t/C_0) \sim t$  plots and presented in Fig. 5c. It is found that when metal halide lamp was used as the visible light source with a cutoff filter to cut off the light below 420 nm, all of the 1D AgBr/BiPO<sub>4</sub> photocatalysts exhibit better photocatalytic activities for MB degradation than the pure BiPO<sub>4</sub> and AgBr. With the 1D rod-like 10.0at%AgBr/BiPO<sub>4</sub> as photocatalyst, the photodegradation rate of MB reaches nearly 100% after 30min of visible-light irradiation, which is much higher than that the others AgBr/BiPO<sub>4</sub> heterostructure, pure- AgBr and BiPO<sub>4</sub>. Following the first-order kinetics model, the determined reaction rate

constant,  $k$ , for the rod-like 0.1at% AgBr/BiPO<sub>4</sub> heterostructure was much higher than about 3-fold as fast as that of pure-BiPO<sub>4</sub> (0.0448 min<sup>-1</sup>) (Fig.5c). Above result indicated that AgBr/BiPO<sub>4</sub> exhibited higher efficiency than that of BiPO<sub>4</sub>. As the reduction of chemical oxygen demand (COD) reflects the extent of degradation or mineralization of an organic species along with the color removal,<sup>50</sup> the change of COD values in the photodegradation of MB with the sample of pure-BiPO<sub>4</sub> and 10at% AgBr/BiPO<sub>4</sub> were studied as a function of irradiation time under visible light, as shown in Fig. 5d. The initial COD concentration of the MB solution is 52.54 mg·L<sup>-1</sup>. After visible-light irradiation for 35min, the COD concentration decreased to 6.36 mg·L<sup>-1</sup>. The significant decrease in the COD values further confirms that MB was truly photodegraded by the AgBr/BiPO<sub>4</sub> heterostructure. Fig. 6 showed the photodegradation of phenol molecules in water. It can be seen that the adsorption of AgBr/BiPO<sub>4</sub> composites were slight worse than pure-BiPO<sub>4</sub>. The photocatalytic activity is enhanced gradually with the proportion of AgBr increasing. When the ratio reaches to 50at%, the as-prepared photocatalyst has an optimal activity. As AgBr also acts as a semiconductor producing electron and hole, increase of its content enhances the photocatalytic activity of AgBr/BiPO<sub>4</sub>. Hence a higher charge carrier concentration was formed between AgBr and BiPO<sub>4</sub> and then improves the photodegradation

efficiency of pure phase. From Fig.6d, the COD removal rate of phenol, we can see that the COD removal rate of 50at% AgBr/BiPO<sub>4</sub> reach nearly 70% relate to that of pure- BiPO<sub>4</sub> just reach 59% under visible light irradiated 25min, therefore for the extent of degradation or mineralization of phenol of 50at% AgBr/BiPO<sub>4</sub> was higher than that of pure-BiPO<sub>4</sub>. The photocatalytic activities of the AgBr/BiPO<sub>4</sub> enhanced remarkably with increasing AgBr content, but higher AgBr loading content, the photocatalytic activity decreased, suggesting that the optimal AgBr content in AgBr/BiPO<sub>4</sub> existed when the molar ratio was 0.1at%. The same phenomenon also reported in other systems.<sup>43, 45-46, 51</sup> The optimum content of AgBr in the heterojunction can be related to the recombination rate of photogenerated electrons and holes. According to literatures reported,<sup>45-46, 51</sup> the space charge region potential for the efficient separation of electron-hole must be certain. When AgBr content was above its optimal vale, the space charge region might become very narrow and the penetration depth of BiPO<sub>4</sub> exceeds the space charge layer, so the recombination of the photogenerated electron-hole pairs in semiconductors become easier. On the other hand, when AgBr content was below its optimal value, the photocatalytic activity was low because fewer electron and hole trapping carriers could be detrimental to the separation of electron-hole pairs.

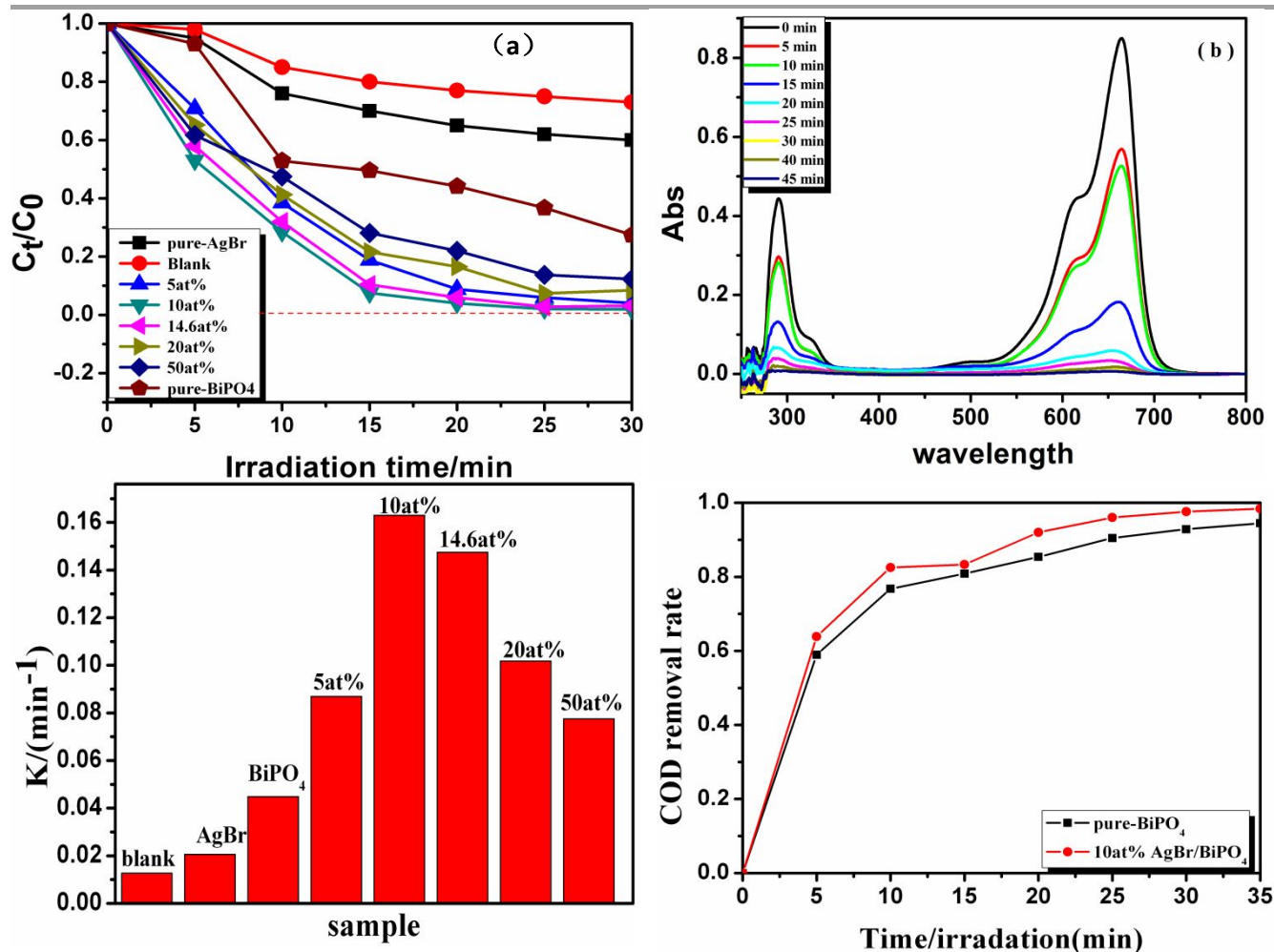
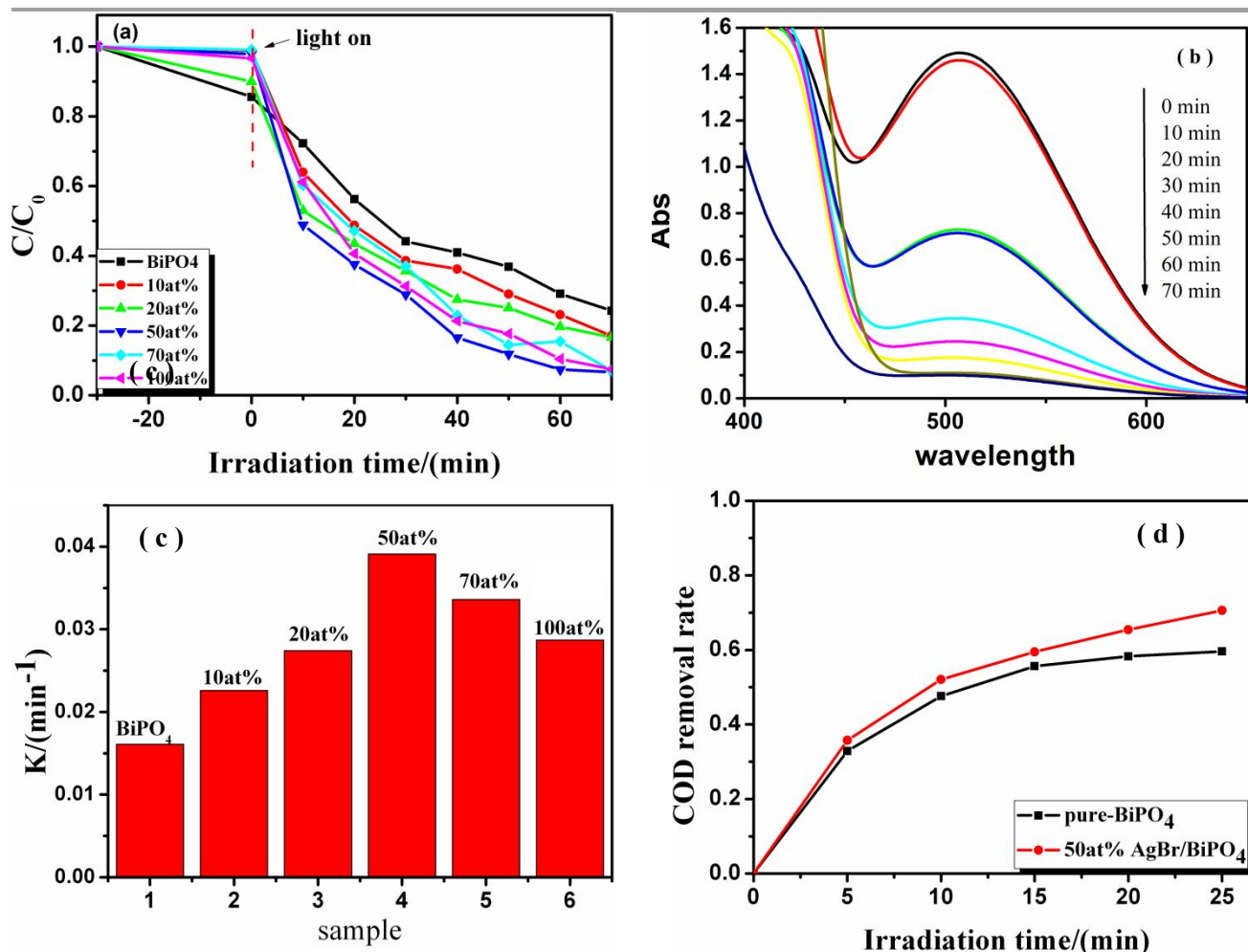


Fig. 5 (a) Photocatalytic properties of BiPO<sub>4</sub> and different AgBr/BiPO<sub>4</sub> catalysts for degrading MB; (b) Concentration change of MB, (c) the comparison of rate constant  $k$ , (d) COD changes during the course of MB photodegradation in the present of pure- BiPO<sub>4</sub>, 10at% AgBr/BiPO<sub>4</sub>.





**Fig. 6** (a) Photocatalytic properties of BiPO<sub>4</sub> and AgBr/BiPO<sub>4</sub> catalysts for degrading phenol. (b) Concentration change of phenol (c) the comparison of rate constant  $k$  (d) COD changes during the course of phenol photodegradation in the presence of pure-BiPO<sub>4</sub> and 50at% AgBr/BiPO<sub>4</sub> heterojunction.

### 3.5 The enhanced photocatalytic activity mechanism of AgBr/BiPO<sub>4</sub> heterojunction

Photoinduced oxide radicals, hydrogen peroxide, and hole were considered as the main oxidizing species in semiconductor photocatalytic processes. To ascertain radicals in this system, *t*-butanol (*t*-BuOH), Ethylene diamine tetraacetic acid (EDTA), and benzoquinone (BQ) were used as scavengers to examine  $\cdot\text{OH}$ ,  $\text{O}_2^{\cdot-}$  and holes, respectively. As shown in Fig. 7, *t*-BuOH and EDTA almost have no effect on AgBr/BiPO<sub>4</sub> photodegradations, which indicate that  $\cdot\text{OH}$  and hole play a negligible role on the photodegradations of AgBr/BiPO<sub>4</sub>. However, the presence of BQ significantly inhibits these degradation reactions, implying the  $\text{O}_2^{\cdot-}$  is crucial effect of on the photocatalytic systems. It's known that BQ has the potential to trap superoxide anions by an electron transfer mechanism (eq. 1)<sup>52-53</sup>:  $\text{BQ} + \text{O}_2^{\cdot-} \rightarrow \text{BQ}^{\cdot-} + \text{O}_2$  (1)

According to the results mentioned above, it can be speculated that the  $\text{O}_2^{\cdot-}$  may be the main active species in the AgBr/BiPO<sub>4</sub> system. We also can explain the photocatalytic enhancement mechanism by employing the electrical impedance spectra (EIS), as shown in Fig. 8. The EIS of the three cathodes both consist of one semicircle in the high frequency region and a sloping line in the

low frequency region, which indicates the double-layer response at the electrode sample interface and the diffusion of lithium ions in the solid matrix.<sup>53</sup> The EIS show BiPO<sub>4</sub> curve of the impedance spectrum (Fig. 8a) of high-frequency semicircle diameter is larger,

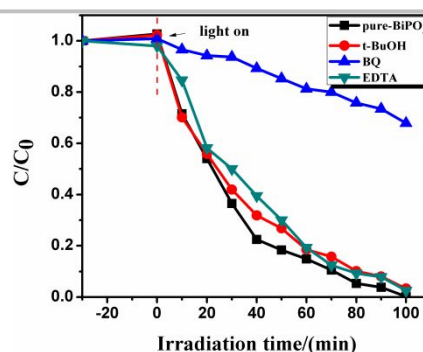


**Fig. 7** Effect of different scavengers on the photocatalytic activity of AgBr/BiPO<sub>4</sub> photocatalyst under visible light irradiation (Concentration of all scavengers were  $5 \times 10^{-3} \text{ mol} \cdot \text{L}^{-1}$ ; Concentration MB is  $10.0 \text{ mg} \cdot \text{L}^{-1}$ ).



it is 2088  $\Omega$  Ret. When the load ratio of AgBr (curve b), the Ret is smaller than bismuth phosphate, when load ratio is 0.5 at %, which Ret is 1688  $\Omega$ , And 0.1 at %, the Ret value is 1381  $\Omega$ , therefore suggests that when AgBr/BiPO<sub>4</sub> loaded ratio was 0.1 at %, which can further promote electron transfer efficiency, and slow down the efficiency of electrons and holes combination in the compounds.

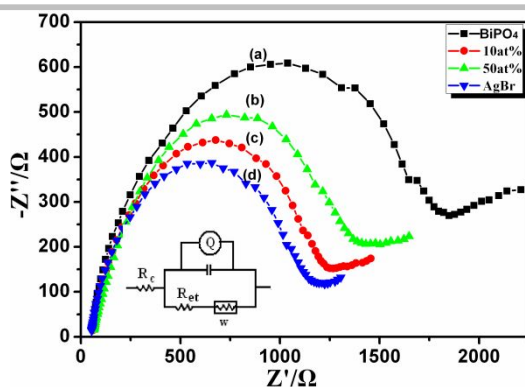


**Fig. 8** Electrical impedance spectra (EIS) patterns of as-obtained samples.

**Table 1** Electrical impedance of as-prepared samples.

	BiPO <sub>4</sub>	10at%AgBr/ BiPO <sub>4</sub>	50at%AgBr /BiPO <sub>4</sub>	AgBr
R <sub>c</sub> ( $\Omega$ )	59.26	61.26	67.54	55.26
R <sub>et</sub> ( $\Omega$ )	2088	1381	1688	1261

Thus, a certain amount of loaded AgBr can increase the photocatalytic activity in the complexes.

To understand the decreased UV-light photocatalytic activity of AgBr/BiPO<sub>4</sub> heterojunction, it is important to explore its photocatalytic mechanism. The VB and CB potentials of BiPO<sub>4</sub> at the point of zero charge can be calculated using the following formulation:<sup>53</sup>

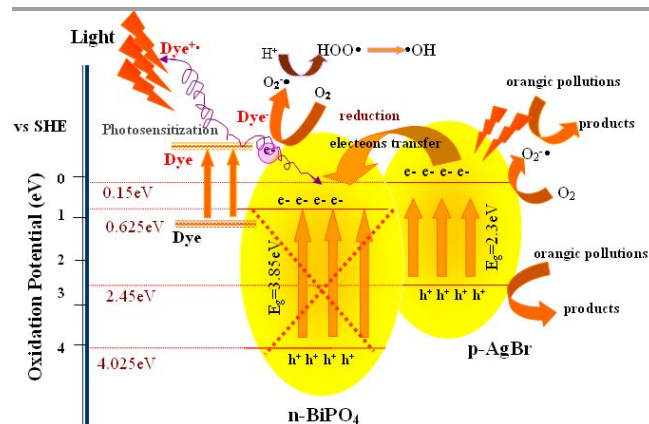
$$E_{VB} = X - E^{\ominus} + 0.5E_g$$

$$E_{CB} = E_{VB} - E_g$$

where  $X$  is the absolute electronegativity of BiPO<sub>4</sub>,  $E^{\ominus}$  is the energy of the free electrons on the hydrogen scale (4.5 eV) and  $E_g$  is the band gap of semiconductors. Based on the above equations, the  $E_g$  values of AgBr and BiPO<sub>4</sub> were calculated to be 2.3eV and 3.85eV, and then their homologous  $E_{CB}$  values were estimated to be 0.15eV and 0.625eV, respectively. The above results suggest that AgBr and BiPO<sub>4</sub> possessed a nested band structure, not the best interactive structure, which seems to be unfavorable for the separation of the photoinduced carriers. Many researchers proposed that the electrons could be excited from the top of the VB to the higher CB positions besides to the bottom positions of the photocatalysts<sup>54-60</sup>. Thus, an ideal interactive energy band structure could be formed. As for the AgBr/BiPO<sub>4</sub> composite, only AgBr could be activated under visible light. When the wavelength was longer than 500 nm, the electrons could migrate from the top of the VB (2.45 eV) to higher CB positions (0.15 eV), then move to the empty bottom of the CB of BiPO<sub>4</sub> (0.625 eV). Finally O<sub>2</sub> molecules adsorbed on the surface of the composite reacted with electrons to produce  $\cdot O_2^-$  that could decompose organic pollutant. Meanwhile, the photogenerated holes on the VB of AgBr could degrade organic pollutant directly. Therefore, the photogenerated electron-hole pairs separated efficiently across the interface between BiPO<sub>4</sub> and AgBr, which results in the enhanced photocatalytic activity of AgBr/BiPO<sub>4</sub>, as shown in Scheme 1. In view of the other

composites<sup>61-64</sup>, it is reasonable that MB may display a weak photosensitization effect on AgBr/BiPO<sub>4</sub> under visible light.

The stability of the catalyst is important for its application. To demonstrate the potential applicability of AgBr/BiPO<sub>4</sub> heterojunction, the stability of 10.0at%AgBr/BiPO<sub>4</sub> was investigated. Fig. 9 shows the results of a repeated experiment for the durability of MB degradation on 10.0at%AgBr/BiPO<sub>4</sub> photocatalyst. It can be seen that after six cycles no obvious activity decrease for 10at%AgBr/BiPO<sub>4</sub> occurs (Fig. 9a), and also no appreciable change in phase has been observed after the catalytic reaction, which implies that the catalysts are rather stable (Fig. 9b).



**Scheme 1** Mechanism for the photocatalytic activity enhancement of AgBr/BiPO<sub>4</sub> heterojunction.

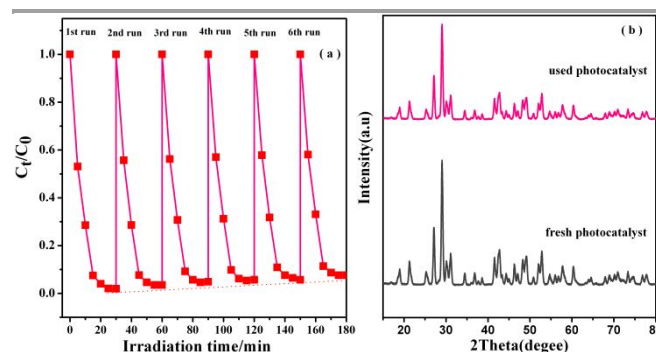


**Fig. 9** (a) The repeated experiments of photocatalytic degradation of MB on the 10.0at%AgBr/BiPO<sub>4</sub> heterojunction under visible light irradiation and XRD patterns of 10.0at%AgBr/BiPO<sub>4</sub> before and after used for five cycles (b).

## 4. Conclusions

In summary, a highly effective visible-light-driven photocatalyst of AgBr/BiPO<sub>4</sub> were successfully prepared via a facile and simple hydrothermal method, which based on a formation of a heterojunction interface AgBr and BiPO<sub>4</sub>. The novel AgBr/BiPO<sub>4</sub> heterostructure exhibited a superior photocatalytic performance compared with the pure phases of AgBr and BiPO<sub>4</sub> for the degradation of MB and phenol. The formation of the AgBr/BiPO<sub>4</sub> heterojunction played a vital role in the efficient separation of electrons and holes for the enhancement of photocatalytic activity. The remarkable enhancement in the photocatalytic performance of AgBr/BiPO<sub>4</sub> is ascribed mainly to the electric-field-driven electron-hole separations at the interface and in the two semiconductors. Besides, the fair mobility for

electron and hole transportation in AgBr and BiPO<sub>4</sub>, respectively, are also favorable for the high photocatalytic property.

## Acknowledgment

This work was supported by the National Natural Science Foundation of China (21373159). This work was also financially supported by the Open Foundation of Key Laboratory of Synthetic and Natural Functional Molecule Chemistry (Ministry of Educational) (338080055) and Project of Science & Technology Office of Shanxi Province (2015SF291, 2013K11-08, 2013SZS20-P01) and Natural Science Program of Education Department of Shaanxi Province (13JK0669).

## References

- L. S. Zhang, H. L. Wang, Z. G. Chen, P. K. Wong and J. S. Liu, *Appl. Catal. B: Environ.*, 2011, **106**, 1–13.
- J. Su, X. X. Zou, G. D. Li, X. Wei, C. Yan, Y. N. Wang, J. Zhao, L. J. Zhou and J. S. Chen, *J. Phys. Chem. C* 2011, **115**, 8064–8071.
- S.N. Chai, G. H. Zhao, Y. N. Zhang, Y. J. Wang, F. Q. Nong, M. F. Li, and D.M. Li, *Environ. Sci. Technol.*, 2012, **46**, 10182–10190.
- G. S. Li, B. Jiang, X. Li, Z. C. Lian, S. N. Xiao, J. Zhu, D. Q. Zhang and H. X. Li, *Appl. Mater. Interfaces*, 2013, **5**, 7190–7197.
- X. B. Chen, Y. B. Lou, A. C. S. Samia, C. Burda and J. L. Gole, *Adv. Funct.*, 2005, **15**, 41–49.
- K. Nakata and A. Fujishima, *J. Photochem. Photobio. C* 2012, **13**, 169–189.
- J. Y. Zhang, H. L. Zhu, S. K. Zheng, F. Pan, and T. M. Wang, *Appl. Mater. Interfaces*, 2009, **10**, 2111–2114.
- V. Etacheri, G. Michlits, M. K. Seery, S. J. Hinder, and S. C. Pillai, *ACS Appl. Mater. Interfaces*, 2013, **5**, 1663–1672.
- A. D. Paola, E. Garcia-López, G. Marci and L. Palmisano, *J. Hazard. Mater.*, 2012, **211**, 3–29.
- R. Dietmueller, H. Nesswetter, S. J. Schoell, I. D. Sharp and M. Stutzmann, *Appl. Mater. Interfaces*, 2011, **3**, 4286–4291.
- H.C. Qin, W. Y. Li, Y. J. Xia and T. He, *Appl. Mater. Interfaces*, 2011, **3**, 3152–3156.
- X.C. Song, Y. F. Zheng, R. Ma, Y.Y. Zhang, H and Y. Yin, *J. Hazard. Mater.*, 2011, **192**, 186–191.
- X. N. Li, R. K. Huang, Y.H. Hu, Y. J. Chen, W. J. Liu, R. S. Yuan and Z. H. Li, *Inorg. Chem.*, 2012, **51**, 6245–6250.
- T. P. Xie, C. L. Liu, L. J. Xu, J. Yang and W. Zhou, *J. Phys. Chem. C* 2013, **117**, 24601–24610.
- N. Zhang, R. Ciriminna, M. Pagliaro, and Y. J. Xu, *Chem. Soc. Rev.*, 2014, **43**, 5276–5287.
- M. L. Zhao, G. S. Li, L. P. Li, L. S. Yang, and J. Zheng, *Cryst. Growth Design*, 2012, **12**, 3983–3991.
- Y. H. Lv, Y. Y. Zhu, and Y. F. Zhu, *J. Phys. Chem. C*, 2013, **117**, 18520–18528.
- M. Ruwet, S. Ceckiewicz and B. Delmon, *Ind. Eng. Chem. Res.*, 1987, **26**, 1981–1983.
- Y. J. Wang, X. F. Guan, L. P. Li and G. S. Li, *CrystEngComm*, 2012, **14**, 7907–7914.
- C. S. Pan, D. Li, X. G. Ma, Y. Chen and Y. F. Zhu, *Catal. Sci. Technol.*, 2011, **1**, 1399–1405.
- J. Geng, W.H. Hou, Y.N. Lv, J. J. Zhu, and H.Y. Chen, *Inorg. Chem.*, 2005, **44**, 8503–8509.
- V. Chandrasekhar, R. K. Metre and R. S. Narayanan, *Dalton Trans.*, 2013, **42**, 8709–8716.
- Q. Y. Zhang, H. Tian, N. Li, M. D. Chen and F. Teng, *CrystEngComm*, 2014, **16**, 8334–8339.
- A. I. Becerro, J. Criado, L. C. Gontard, S. Obregón, A. Fernández, G. Colón, and M. Ocaña, *Cryst. Growth Des.*, 2014, **14**, 3319–3326.
- Y. H. Lv, Y. F. Liu, Y. Y. Zhu and Y. F. Zhu, *J. Mater. Chem. A*, 2014, **2**, 1174–1182.
- S. N. Achary, D. Errandonea, A. Muñoz, P. Rodríguez-Hernández, F. J. Manjón, P. S. R. Krishna, S. J. Patwe, V. Grover and A. K. Tyagi, *Dalton Trans.*, 2013, **42**, 14999–15015.
- C. S. Pan and Y. F. Zhu, *Environ. Sci. Technol.*, 2010, **44**, 5570–5574.
- C. S. Pan and Y. F. Zhu, *J. Mater. Chem.*, 2011, **21**, 4235–4241.
- W. Z. Wang, X.W. Huang, S. Wu, Y.X. Zhou, L.J. Wang, H. L. Shi, Y. J. Liang and B. Zou, *Appl. Catal. B: Environ.*, 2013, **134**, 293–301.
- P. Arunkumar, C. Jayajothi, D. Jeyakumar and N. Lakshminarasimhan, *RSC Adv.*, 2012, **2**, 1477–1485.
- M. L. Zhao, L. P. Li, J. Zheng, L. S. Yang, and G. S. Li, *Inorg. Chem.*, 2013, **52**, 807–815.
- M. L. Zhao, G. S. Li, J. Zheng, L. P. Li, H. Wang and L. S. Yang, *CrystEngComm*, 2011, **13**, 6251–6257.
- M. Y. Guan, J. H. Sun, F. F. Tao and Z. Xu, *Cryst. Growth Des.*, 2008, **8**, 2694–2697.
- Z. Wang, J. Feng, M. Pang, S. H. Pan and H. J. Zhang, *Dalton Trans.*, 2013, **42**, 12101–12108.
- Y. Y. Zhang, H. Q. Fan, M. M. Li and H. L. Tian, *Dalton Trans.*, 2013, **42**, 13172–13178.
- M. H. Fulekar, A. Singh, D. P. Dutta, Mainak Roy, Anand Ballal and A. K. Tyagi, *RSC Adv.*, 2014, **4**, 10097–10107.
- T. Lv, L. K. Pan, X. J. Liu and Z. Sun, *RSC Adv.*, 2012, **2**, 12706–12709.
- E. P. Gao and W. Z. Wang, *Nanoscale*, 2013, **5**, 11248–11256.
- Z. S. Li, B. L. Li, S. H. Peng, D. H. Li, S. Y. Yang and Y. P. Fang, *RSC Adv.*, 2014, **4**, 35144–35148.
- H. L. Lin, H. F. Ye, S. F. Chen and Y. Chen, *RSC Adv.*, 2014, **4**, 10968–10974.
- G. S. Liu, S. W. Liu, Q. F. Lu, H. Y. Sun, and Z. L. Xiu, *Ind. Eng. Chem. Res.*, 2014, **53**, 13023–13029.
- H. Xu, Y. G. Xu, H. M. Li, J. X. Xia, J. Xiong, S. Yin, C. J. Huang and H. L. Wan, *Dalton Trans.*, 2012, **41**, 3387–3394.
- D. J. Wang, L. Guo, Y. Z. Zhen, L. L. Yue, G. L. Xue, and F. Fu, *J. Mater. Chem. A*, 2014, **2**, 11716–11727.
- H. F. Cheng, B. B. Huang, P. Wang, Z. Y. Wang, Z.Z. Lou, J. P. Wang, X. Y. Qin, X. Y. Zhang and Y. Dai, *Chem. Commun.*, 2011, **47**, 7054–7056.
- C. Hu, Y. Q. Lan, J. H. Qu, X. X. Hu and A. M. Wang, *J. Phys. Chem. B*, 2006, **110**, 4066–4072.
- H. Zhang, G. Wang, D. Chen, X. J. Lv and J. H. Li, *Chem. Mater.*, 2008, **20**, 6543–6549.
- H. L. Lin, J. Cao, B. D. Luo, X. B. Yan and S. F. Chen, *Chin. Sci. Bull.*, 2012, **57**, 2901–2907.
- P. Chen, Y. Su, H. Liu and Y. Wang, *ACS Appl. Mater. Interfaces*, 2013, **5**, 12073–12082.
- B. A. Hu, X. Y. Wang, Q. L. Wei, H. B. Shu, X. K. Yang, Y. S. Bai, H. Wu, Y. F. Song and L. Liu, *J. Alloys. Compounds*, 2013, **579**, 18–26.
- M. Shang, W. Z. Wang, L. Zhang, S. M. Sun, L. Wang, and L. Zhou, *J. Phys. Chem. C* 2009, **113**, 14727–14731.
- O. Lupan, L. Chow, L. K. Ono, B. R. Cuenya, G. Y. Chai, H. Khallaf, S. Park and A. Schulte, *J. Phys. Chem. C*, 2010, **114**, 12401–12408.
- P. Qu, J. Zhao, T. Shen and H. Hidaka, *J. Mol. Catal. A: Chem.* 1998, **129**, 257–268.
- J. H. Kou, Z. S. Li, Y. P. Yuan, H. T. Zhang, Y. Wang and Z. G. Zhou, *Environ. Sci. Technol.*, 2009, **43**, 2919–2924.
- H. L. Wang, L. S. Zhang, Z. G. Chen, J. Q. Hu, S. J. Li, Z. H. Wang, J. S. Liu and X. C. Wang, *Chem. Soc. Rev.*, 2014, **43**, 5234–5244.
- X. Zhang, L. Z. Zhang, T. F. Xie and D. J. Wang, *J. Phys. Chem. C* 2009, **113**, 7371–7378.
- L. Q. Ye, J. N. Chen, L. H. Tian, J. Y. Liu, T. Y. Peng and K. J. Deng, *Appl. Catal. B: Environ.*, 2013, **130**, 1–7.
- Y. Y. Li, J. S. Wang, H. C. Yao, L. Y. Dang and Z. J. Li, *J. Mol. Catal. A: Chem.*, 2011, **334**, 116–122.
- T. B. Li, G. Chen, C. Zhou, Z. Y. Shen, R. C. Jin and J. X. Sun, *Dalton Trans.*, 2011, **40**, 6751–6758.
- J. Cao, B. Y. Xu, H. Lin, B. D. Luo and S. F. Chen, *Chem. Eng. J.*, 2012, **185**, 91–99.
- Y. Y. Li, J. S. Wang, H. C. Yao, L. Y. Dang and Z. J. Li, *Catal. Commun.*, 2011, **12**, 660–664.
- X. J. Wang, W. Y. Yang, F. T. Li, Y. B. Xue, R. H. Liu, and Y. J. Hao, *Ind. Eng. Chem. Res.*, 2013, **52**, 17140–17150.
- C. Zhang, Y. F. Zhu, *Chem. Mater.*, 2005, **17**, 3537–3545.
- W. R. Zhao, Y. Wang, Y. Yang, J. Tang and Y. N. Yang, *Appl. Catal. B: Environ.*, 2012, **115**: 90–99.
- W. Z. Wang, X.W. Huang, S. Wu, Y. X. Zhou, L.J. Wang, H. L. Shi, Y. J. Liang and B. Zou, *Appl. Catal. B: Environ.*, 2013, **134**, 293–301.

## Graphical abstract

AgBr nanoparticles were decorated on the surface of BiPO<sub>4</sub> micro-rod to fabricate a novel p-n heterojunction photocatalyst *via* a facile deposition-precipitation method.

